

1                    **Storms and the Depletion of Ammonia in Jupiter:**  
 2                    **II. Explaining the Juno observations**

3                    **Tristan Guillot<sup>1,2</sup>, Cheng Li<sup>3,4</sup>, Scott J. Bolton<sup>5</sup>, Shannon T. Brown<sup>6</sup>, Andrew**  
 4                    **P. Ingersoll<sup>3</sup>, Michael A. Janssen<sup>6</sup>, Steven M. Levin<sup>6</sup>, Jonathan I. Lunine<sup>7</sup>,**  
 5                    **Glenn S. Orton<sup>6</sup>, Paul G. Steffes<sup>8</sup>, David J. Stevenson<sup>3</sup>**

6                    <sup>1</sup>Université Côte d'Azur, OCA, Lagrange CNRS, 06304 Nice, France

7                    <sup>2</sup>The University of Tokyo, Department of Earth and Planetary Science, Tokyo 113-0033, Japan

8                    <sup>3</sup>California Institute of Technology, Pasadena, CA 91125, USA

9                    <sup>4</sup>University of California Berkeley, USA

10                  <sup>5</sup>Southwest Research Institute, San Antonio, Texas, USA

11                  <sup>6</sup>Jet Propulsion Laboratory, California Institute of Technology, Pasadena, CA 91109, USA

12                  <sup>7</sup>Cornell University, Ithaca, New York 14853, USA

13                  <sup>8</sup>School of Electrical and Computer Engineering, Georgia Institute of Technology, Atlanta, GA, USA

14                  **Key Points:**

- 15                  • Juno measurements show that ammonia gas in Jupiter has variable abundance
- 16                  to great depth and as a function of latitude
- 17                  • We show that Jupiter's powerful storms control ammonia abundance by lead-
- 18                  ing to the formation of water-ammonia hailstones (mushballs) and evaporative
- 19                  downdrafts
- 20                  • A simple atmospheric mixing model successfully links measured lightning rate
- 21                  to ammonia abundance and predicts variable water abundance to great depth.

---

Corresponding author: Tristan Guillot, [tristan.guillot@oca.eu](mailto:tristan.guillot@oca.eu)

22 **Abstract**

23 Observations of Jupiter’s deep atmosphere by the Juno spacecraft have revealed several  
 24 puzzling facts: The concentration of ammonia is variable down to pressures of tens  
 25 of bars, and is strongly dependent on latitude. While most latitudes exhibit a low  
 26 abundance, the Equatorial Zone of Jupiter has an abundance of ammonia that is high  
 27 and nearly uniform with depth. In parallel, the Equatorial Zone is peculiar for its  
 28 absence of lightning, which is otherwise prevalent most everywhere else on the planet.  
 29 We show that a model accounting for the presence of small-scale convection and water  
 30 storms originating in Jupiter’s deep atmosphere accounts for the observations. Where  
 31 strong thunderstorms are observed on the planet, we estimate that the formation of  
 32 ammonia-rich hail (‘mushballs’) and subsequent downdrafts can deplete efficiently the  
 33 upper atmosphere of its ammonia and transport it efficiently to the deeper levels.  
 34 In the Equatorial Zone, the absence of thunderstorms shows that this process is not  
 35 occurring, implying that small-scale convection can maintain a near-homogeneity of  
 36 this region. A simple model satisfying mass and energy balance accounts for the  
 37 main features of Juno’s MWR observations and successfully reproduces the inverse  
 38 correlation seen between ammonia abundance and the lightning rate as function of  
 39 latitude. We predict that in regions where ammonia is depleted, water should also be  
 40 depleted to great depths. This new vision of the mechanisms at play, which are both  
 41 deep and latitude-dependent, has consequences for our understanding of Jupiter’s deep  
 42 interior and of giant-planet atmospheres in general.

43 **Plain Language Summary**

44 Measurements by the Juno spacecraft have shown that ammonia in Jupiter is  
 45 present near the equator of the planet but is depleted to great depths at other latitudes,  
 46 something never anticipated by theoretical models. In a companion paper, we showed  
 47 that ammonia can combine to water to form hail-like particles (mushballs) that can  
 48 fall to great depths. Here we show that storms can indeed effectively deplete the  
 49 upper atmosphere to great depths. The dichotomy seen with the ammonia abundance  
 50 between the equator and other regions is also seen in the measured flash rate, indicative  
 51 of storm activity in Jupiter: No lightning has been detected at the equator in the region  
 52 which has a high abundance of ammonia. We predict that water, another crucial  
 53 species to understand Jupiter’s meteorology and formation, is also depleted to great  
 54 depths. Thus Jupiter’s atmosphere is much more complex than anticipated, affecting  
 55 how we understand its interior, composition and formation. This should also apply to  
 56 other giant planets, and to exoplanets with hydrogen atmospheres.

57 **1 Introduction**

58 Jupiter is the archetype of planets with deep hydrogen atmospheres. Contrary  
 59 to the Earth, it has no surface and all condensates are heavier than the main non-  
 60 condensable constituents, hydrogen and helium. Recent observations reveal that its  
 61 atmosphere is much more complex than traditionally assumed, with implications for  
 62 its dynamics, the structure and internal composition of Jupiter and the evolution of  
 63 planets with hydrogen atmospheres, including exoplanets.

64 Jupiter is known for its alternance of dark reddish-zones and light, white belts.  
 65 Besides their colors, these zones and belts are characterized by alternating zonal speeds  
 66 that differ by up to about 100 m/s (García-Melendo & Sánchez-Lavega, 2001; Porco  
 67 et al., 2003; Tollefson et al., 2017). But when observed at much longer wavelengths  
 68 (1 to 60 cm), the Juno microwave radiometer (MWR) sees a different structure: An  
 69 equatorial region between latitudes 0° and 5°N which is systematically colder (lower  
 70 brightness temperature) than all other latitudes and fainter variations between zones  
 71 and belts (Bolton et al., 2017). This reveals a puzzling dichotomy of Jupiter’s deep

72 atmosphere: In this  $0^\circ - 5^\circ\text{N}$  latitudinal region, the atmosphere contains a high,  
 73 vertically relatively uniform, abundance of ammonia whereas it is much lower and  
 74 variable at other latitudes (C. Li et al., 2017). The abundance of ammonia increases  
 75 with depth and may become equal to the equatorial value, but at pressures of 30 bars  
 76 or more (C. Li et al., 2017).

77 Signs of the depletion of ammonia in Jupiter’s atmosphere were obtained from  
 78 ground-based radio-wave observations as early as 1986 (de Pater, 1986; de Pater et  
 79 al., 2001, 2019) but the observations could not probe levels as deep as those accessible  
 80 to Juno. The dichotomy between the equatorial region and other latitudes is also  
 81 seen in the  $5\text{-}\mu\text{m}$  spectroscopic observations of Jupiter at 1-4 bar levels, although the  
 82 retrieval is more complex due to the effects of clouds (Giles et al., 2017; Blain et  
 83 al., 2018). This dichotomy cannot be explained solely by meridional circulation (e.g.  
 84 upward motion at the equator and downward motion at other latitudes) and requires a  
 85 localized downward transport of ammonia that is essentially invisible to Juno’s MWR  
 86 instrument (Ingersoll et al., 2017). We must therefore seek a process capable of (i)  
 87 drying the upper atmosphere of its ammonia to great depths, (ii) accounting for the  
 88 dichotomy between the equatorial region and other latitudes while (iii) remaining  
 89 sufficiently small-scale and/or intermittent to have escaped detection thus far.

90 In a companion paper (hereafter paper I), we have shown that during strong  
 91 storms able to loft water ice into a region located at pressures between 1.1 and 1.5 bar  
 92 and temperatures between 173K and 188K, ammonia vapor can dissolve into water ice  
 93 to form a low-temperature liquid phase containing about 1/3 ammonia and 2/3 water.  
 94 The subsequent formation of ammonia-rich hail that we call ‘mushballs’ leads to an  
 95 effective transport of the ammonia to deep levels (between 7 and 25 bars, depending  
 96 on poorly-known ventilation coefficients). Further sinking of ammonia- and water-rich  
 97 plumes must take place because evaporation leads to a gas that has a high molecular  
 98 weight and a low temperature due to evaporative cooling.

99 This downward transport is a necessary but not sufficient condition to explain the  
 100 observations: It can be argued that storms, particularly strong storms, cover a tiny  
 101 fraction of the atmosphere of the planet and they are strongly intermittent. Based  
 102 on our experience of Earth’s storms, hail is rare (fortunately!). Lastly, mass balance  
 103 implies that some of the ammonia-rich atmosphere from the deeper level must be  
 104 transported upward. Given these observations how could hail (or mushball) formation  
 105 be of significance in Jupiter?

106 The present paper explores the consequences of the presence of mushballs and  
 107 evaporative downdrafts for the atmosphere of Jupiter. Can such a process operate  
 108 efficiently enough to yield a widespread depletion of ammonia in most of Jupiter’s  
 109 troposphere? Can it account for the main features of Juno/MWR measurements?  
 110 What are its consequences for our understanding of Jupiter’s atmospheric heat engine  
 111 and for the distribution of water on the planet? We propose hereafter a simple local  
 112 model to address these questions broadly, leaving aside for future work other important  
 113 aspects like time-dependency and interplay between local vertical transport and global  
 114 mixing.

115 The paper is organized as follows: In Section 2, we put the Juno MWR maps  
 116 of inferred ammonia abundance in the context of a physical model of Jupiter’s deep  
 117 atmosphere. In Section 3, we then present a toy model that solves mass- and energy-  
 118 balance locally in Jupiter. We apply this model to interpret the MWR observations and  
 119 derive consequences for our understanding of Jupiter’s deep atmosphere in Section 4.

120 **2 Juno’s ammonia abundance map**

121 The Juno microwave radiometer measures the thermal radiation of Jupiter’s at-  
 122 mosphere at six radio wavelengths probing approximately from 0.7 to 250 bars. Be-  
 123 cause Jupiter is emitting more heat than it receives from the Sun (Hanel et al., 1981;  
 124 L. Li et al., 2018) and because radiative opacities are large (Guillot et al., 1994, 2004)  
 125 it is believed that its deep atmosphere (below the ammonia condensation level) should  
 126 be largely convective and adiabatic. This was confirmed within a few kelvins (see  
 127 hereafter Section 3.2) both by radio occultation from the Voyager spacecraft (Lindal  
 128 et al., 1981) and in situ measurements of the Galileo probe (Magalhaes et al., 2002).  
 129 Assuming Jupiter’s temperature profile lies on an adiabat defined by the Galileo mea-  
 130 surement (i.e., 166.1 K at 1 bar), the variations of the brightness temperatures as a  
 131 function of latitude and wavelength are entirely determined by the distribution of the  
 132 ammonia gas, which is the major absorber in the wavelengths of Juno/MWR (Janssen  
 133 et al., 2017). The 2D distribution of ammonia is derived by fitting the microwave  
 134 spectra at every latitude. In C. Li et al. (2017), the map was derived by using only  
 135 the observation of the first perijove (PJ1). The subsequent observations probe dif-  
 136 ferent longitudes and are very similar to PJ1. Therefore, we use the average of the  
 137 first 9 perijoves to produce the mean condition of Jupiter’s atmosphere across multiple  
 138 longitudes.

139 Figure 1 shows that for latitudes between 0° and 5°N, the ammonia concentration  
 140 is high, near its global maximum of 360 ppmv, and mostly uniform with depth. (A  
 141 small increase in the concentration above 360 ppmv near 1-3 bar may be reproduced by  
 142 including the effect of ammonia rain (C. Li & Chen, 2019).) Away from the equator,  
 143 the atmosphere is depleted in ammonia from the higher levels, down to ~ 30 bar or  
 144 so, where it increases to its global maximum. A maximum depletion of ammonia is  
 145 observed between latitudes 5° and 20°N, with an abundance of order 100 ppmv near  
 146 1 bar increasing progressively to reach about 200ppmv near 10 bar. Another local  
 147 minimum with an ammonia abundance below 200 ppmv is located between lat. -12°  
 148 and -18°S, but is limited to pressures smaller than 3 bar. Aside from these regions, the  
 149 ammonia abundance below 10 bars fluctuates with altitude between 200 and 250 ppmv  
 150 and rises progressively to about 360 ppmv at pressures between 30 and 100 bar.

151 These features are shared on all the passes observed with MWR and are thus  
 152 very stable (an exception is the location of the Great Red Spot, which we do not  
 153 consider here). There are fluctuations from one pass to the next but they are limited  
 154 in magnitude and in range. In particular, the Equatorial Zone between 0° and 5°N  
 155 always shows a high nearly uniform abundance of ammonia near 360 ppmv, the region  
 156 between 5° and 20° is always the most depleted down to about 10-20 bar and the  
 157 second minimum at pressures smaller than about 3 bar is always near -16°.

158 For the deeper levels the information in Fig. 1 relies on data from MWR chan-  
 159 nels 2 and 1 whose weighting functions are very broad and peak around 30 bar and  
 160 250 bar, respectively (Janssen et al., 2017). This implies that the pressure at which  
 161 the ammonia abundance starts rising (i.e., 20 bars or so) is uncertain. Also, we cannot  
 162 distinguish between a progressive or sudden change.

163 In order to test whether the formation of mushballs can reproduce the basic fea-  
 164 tures of the Juno MWR map, we build a simple, 5-layer model based on the properties  
 165 of the different regions. From top to bottom, these layers are: (1) the upper atmo-  
 166 sphere, (2) the mushball-forming region, (3) the water-cloud region, (4) the downdraft  
 167 region and (5) the deep interior. Ammonia vapor is present in all regions, but water  
 168 vapor is present only in layers (3), (4) and (5) (it is present as ice in regions (1) and  
 169 (2) but only intermittently).

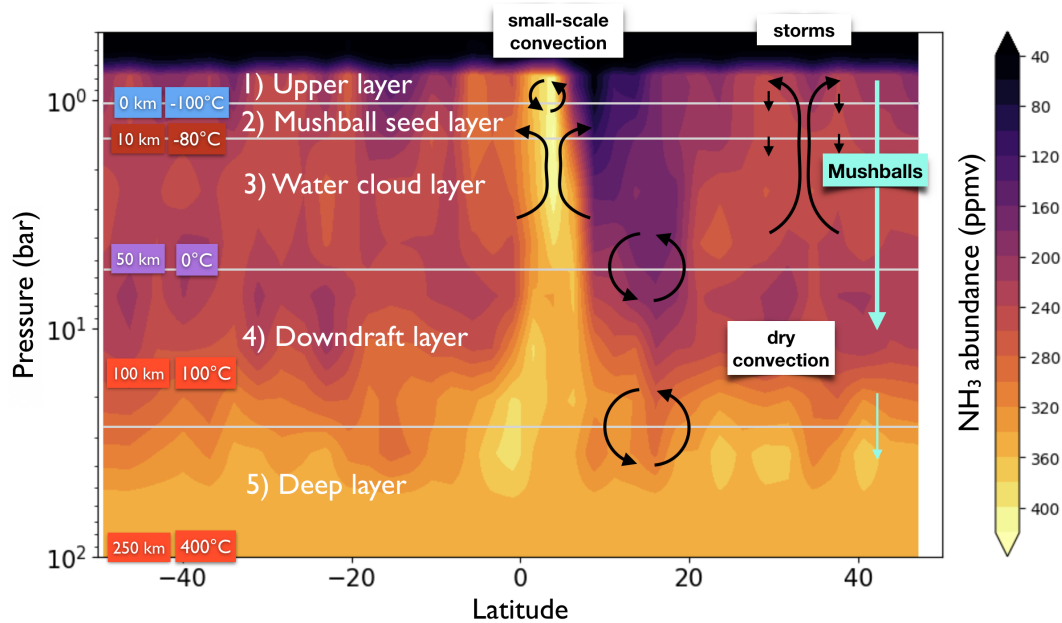


**Figure 1.** Average map of ammonia abundance in Jupiter retrieved by the Juno MWR during PJ1 to PJ9 as a function of latitude and pressure. Overlaid are indications of altitude and temperature as well as the layers and mechanisms (small-scale convection and/or storms in the water condensation region, dry convection deeper) considered in this work (see text). Water vapor condenses to ice particles at  $\sim 5$  bar level ( $0^\circ\text{C}$ ),  $\sim 50$  km below the 1 bar level.

170 We furthermore consider that transport in the water condensation region (layers 3  
 171 to 1) can occur either through small-scale convection or through large water storms. In  
 172 the deeper interior, from layers 5 to 3, transport of interior heat and chemical species  
 173 is done by dry convection. We expect small-scale convection to occur when moist  
 174 convection is inhibited (e.g. because of mass loading or vertical shear). Small-scale  
 175 convection is expected to transport elements and heat across adjacent layers. Rain  
 176 or snow may occur but without any transport of the condensates across the different  
 177 layers. Thunderstorms should occur in the water-cloud region (3) whenever conditions  
 178 are favorable (moist convection is not inhibited). We envision that they should lead  
 179 to an upward transport of ice particles through the mushball-forming region (2) and  
 180 into the upper region (1).

181 On the basis of the observation of a large complex of storms in Jupiter’s atmo-  
 182 sphere by the Galileo mission (Gierasch et al., 2000), we envision that large storms  
 183 should be the dominant mode of heat transport between the water cloud base (3) and  
 184 the top layer (1). The frequency of these storms could be defined by the radiative  
 185 timescale and the requirement to build convective available potential energy (CAPE)  
 186 in order to exceed the buoyancy threshold (C. Li & Ingersoll, 2015). At deeper levels,  
 187 dry convection should occur, possibly powered by deeper “rock storms” created by the  
 188 condensation of silicates and iron (Markham & Stevenson, 2018).

189 Mushballs may form only when ice particles are transported to level (2) (Fig.  
 190 3), i.e. during thunderstorm events. Once formed, we envision that they rain down  
 191 below the water-cloud base, to region (4) where they vaporize and partially to region  
 192 (5) through downdrafts. The mean location of these five layers is set to  $P_1 = 1$  bar,  
 193  $P_2 = 1.3$  bar,  $P_3 = 4$  bar,  $P_4 = 8$  bar and  $P_5 = 20$  bar. While the location of the first  
 194 three layers are set by physical and thermodynamical constraints (the properties of

195 the upper atmosphere, the location of the mushball-formation and water-condensation  
 196 regions), we note that the average pressures for layers 4 and 5 is loosely guided by the  
 197 MWR results but is largely unconstrained at this point.

### 198 3 A toy model for Jupiter’s atmosphere

199 We now develop a simple, toy model of Jupiter’s deep atmosphere. We choose  
 200 an extreme approach, namely to assume that horizontal mixing may be neglected so  
 201 that a steady-state may be achieved at each latitude/longitude in Jupiter. We first  
 202 derive the governing equations of the model, find some analytical solutions and show  
 203 how the ammonia abundance, water abundance and potential temperature vary as a  
 204 function of the frequency of water storms.

#### 205 3.1 Governing equations

206 Let us consider mass and energy balance in our simple 5-layer model shown in  
 207 Fig. 1. We define as  $c_1, \dots, c_5$  the abundances of  $\text{NH}_3$  in the 5 layers,  $w_1, \dots, w_5$  the  
 208 abundances of  $\text{H}_2\text{O}$  (with  $w_1 = w_2 = 0$ ) and  $T_1, \dots, T_5$  their temperatures. We fix the  
 209 bulk (bottom) mixing ratios of  $\text{NH}_3$ ,  $c$ , and water,  $w$ , and impose that the atmosphere  
 210 must transport a known internal heat flux  $F_{\text{tot}}$  (L. Li et al., 2018).

211 We consider storms and convective mixing as discrete events connecting the dif-  
 212 ferent layers. Our approach including all the terms included to calculate the mass  
 213 balance of ammonia and water is shown hereafter in Figs. 2 and 3, respectively. The  
 214 three mechanisms that we envision lead to an upward transport of material per unit  
 215 time  $\delta t$  of a mass  $\dot{m}_{\text{conv}}\delta t$ ,  $\dot{m}_{\text{storm}}\delta t$  and  $\dot{m}_{\text{deep}}\delta t$ , respectively. The same mass is also  
 216 transported downward either as part of the downward convective cell or due to com-  
 217 pensating subsidence. In addition, on the basis of the findings of Paper I, we envision  
 218 that a downward flux of mushballs deliver a mass of ammonia  $c_{\text{mush}}\dot{m}_{\text{storm}}\delta t$  down  
 219 to layer 5, and a mass of water that is split between  $a_w w_{\text{mush}}\dot{m}_{\text{storm}}\delta t$  to layer 4 and  
 220  $(1 - a_w)w_{\text{mush}}\dot{m}_{\text{storm}}\delta t$  to layer 5, with  $a_w$  being a parameter between 0 and 1.

221 The mushball mass flux is parameterized as follows: We consider that the mush-  
 222 ball efficiency mechanism is proportional to the difference between the mixing ratio  
 223 in layer 2 and the minimum mixing ratio for the process to operate,  $\approx 100$  ppmv (see  
 224 Paper I). We also consider that the mushball flux is limited by the amount of water  
 225 present in the water cloud layer,  $w_3$ . The flux itself is proportional to the mass flux  
 226 due to storms. We thus write:

$$\begin{cases} c_{\text{mush}} = \epsilon \min(c_2 - c_{\text{min}}, w_3 f_{\text{NH}_3} / f_{\text{H}_2\text{O}}), \\ w_{\text{mush}} = c_{\text{mush}} f_{\text{H}_2\text{O}} / f_{\text{NH}_3}, \end{cases} \quad (1)$$

227 where  $\epsilon$  is an efficiency parameter ( $0 \leq \epsilon \leq 1$ ) and  $f_{\text{NH}_3}$  and  $f_{\text{H}_2\text{O}}$  are the mass  
 228 mixing ratios of condensed ammonia and water in the mushballs, respectively. Our  
 229 fiducial parameters based on our simple mushball evolution model are  $\epsilon = 0.3$ ,  $f_{\text{NH}_3}$   
 230  $= 0.1$  (thus  $f_{\text{H}_2\text{O}} = 0.9$ ),  $a = 0.5$ .

231 The total downward mushball flux to level 4 is thus

$$\dot{m}_{\text{mush},1 \rightarrow 4} = (c_{\text{mush}} + w_{\text{mush}})\dot{m}_{\text{storm}} = (w_{\text{mush}}/f_{\text{H}_2\text{O}})\dot{m}_{\text{storm}}. \quad (2)$$

232 Where the “ $\sim$ ” sign indicates that only condensates are considered. In addition, some  
 233 air may be entrained down with the mushballs. Let us define  $q_{\text{mush}}$ , the mass fraction  
 234 of mushballs in that downward stream. The upward flux to compensate for the flux  
 235 of mushballs and entrained air is thus:

$$\dot{m}_{1 \rightarrow 4} = \dot{m}_{\text{mush},1 \rightarrow 4} / q_{\text{mush}} \equiv \varpi_{\text{mush}} \dot{m}_{\text{storm}}, \quad (3)$$

236 where  $\varpi_{\text{mush}} = w_{\text{mush}} / (f_{\text{H}_2\text{O}} q_{\text{mush}})$ . We will assume that until mushballs evaporate,  
 237 the fraction of air that is entrained is small, hence  $q_{\text{mush}} \approx 1$ .

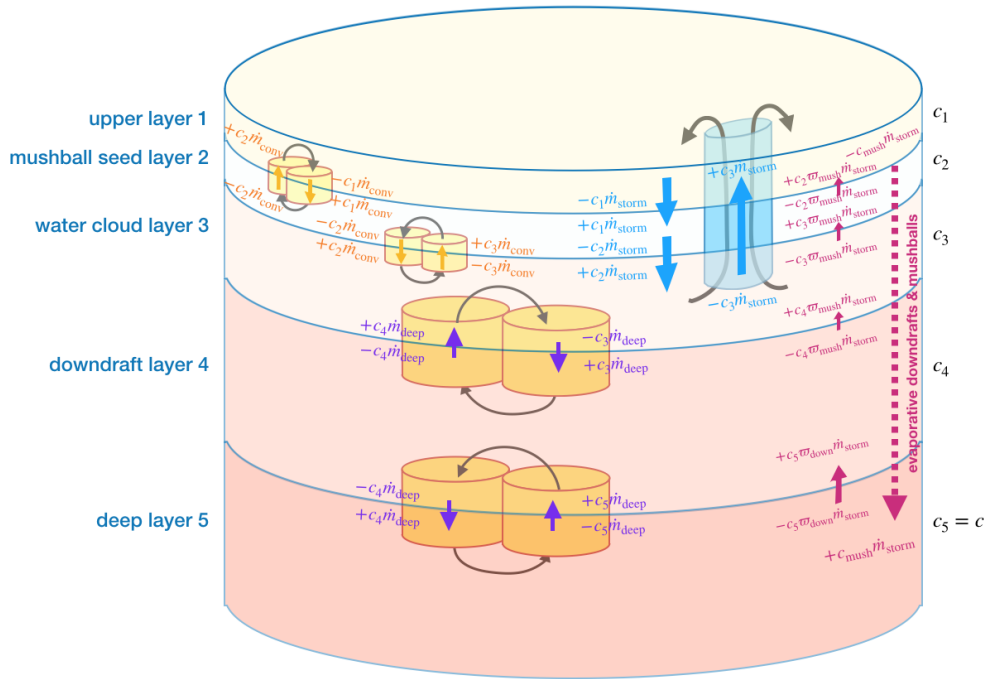


**Figure 2.** Mass balance of ammonia in the framework of our 5-layer model. We consider that three main processes transport material between layers: In yellow, small-scale convection is modeled as an updraft and its reciprocal downdraft between adjacent layers. We consider that it is characterized by an upward mass flux  $\dot{m}_{deep}$  between layers 5 and 4 and layers 4 and 3, and by an upward mass flux  $\dot{m}_{conv}$  between layers 3 and 2 and layers 2 and 1. In blue, strong storms due to water condensation lead to a transport of material directly from layer 3 to layer 1 and to a compensating subsidence mass flux from layer 1 to layer 2 and to layer 3. These storms also lead to the formation of mushballs and evaporative downdrafts which deliver ammonia and water directly to layers 4 and 5. The terms in each layer correspond to the mass balance of ammonia described by Eq. (7).

**Table 1.** Parameters of our global model

Variable	Note	Fiducial value
$c$	Bulk mass mixing ratio of ammonia	0.0027
$w$	Bulk mass mixing ratio of water	0.021
$F_{\text{tot}}$	Internal heat flux	
$\dot{m}_{\text{conv}}$	Upward convective mass flux (layers 2 $\leftrightarrow$ 1 & 3 $\leftrightarrow$ 2)	
$\dot{m}_{\text{storm}}$	Upward mass flux due to water storms (layers 3 $\rightarrow$ 1)	
$\dot{m}_{\text{deep}}$	Upward convective deep mass flux (layers 4 $\leftrightarrow$ 3 & 5 $\leftrightarrow$ 4)	
$a_w$	Fraction of water in mushballs ending in layer 4	0.5
$\epsilon$	Efficiency of mushball formation	0.3
$f_{\text{NH}_3}$	Fraction of NH <sub>3</sub> in mushballs	0.1
$f_{\text{H}_2\text{O}}$	Fraction of H <sub>2</sub> O in mushballs	0.9
$q_{\text{mush}}$	Mass mixing ratio of condensables in downward plumes from levels 1 to 4	1
$q_{\text{down}}$	Mass mixing ratio of condensables in downward plumes from levels 4 to 5	$2w$
$c_1$ to $c_5$	Ammonia mass mixing ratio in layers 1 to 5	
$w_1$ to $w_5$	Water mass mixing ratio in layers 1 to 5	
$s_1$ to $s_5$	Dry static stability in layers 1 to 5	
$\theta_1$ to $\theta_5$	Potential temperature in layers 1 to 5	
$M_1$ to $M_5$	Masses of layers 1 to 5	
$P_1$ to $P_5$	Average pressures of layers 1 to 5	
$c_{\text{mush}}$	Surface-average mixing ratio of ammonia in sinking mushballs	
$w_{\text{mush}}$	Surface-average mixing ratio of water in sinking mushballs	
$\varpi_{\text{mush}}$	See eq. 3	
$\varpi_{\text{down}}$	See eq. 5	
$f_{\text{storm}}$	$\equiv \dot{m}_{\text{storm}}/\dot{m}_{\text{deep}}$	
$f_{\text{conv}}$	$\equiv \dot{m}_{\text{conv}}/\dot{m}_{\text{deep}}$	
$L_v$	Latent heat of vaporization of water (at 0°C)	$2.52 \times 10^{10}$ erg/g

238 Between level 4 and level 5 we consider that part of the mushballs have been  
 239 stripped of their water and that even after full evaporation further sinking proceeds be-  
 240 cause of downdrafts powered by evaporative cooling (see Paper I). The downward flux  
 241 of ammonia is thus  $c_{\text{mush}}\dot{m}_{\text{storm}}$  and the downward flux of water  $(1 - a_w)w_{\text{mush}}\dot{m}_{\text{storm}}$ .  
 242 Thus, the total downward flux of condensates is

$$\dot{m}_{\text{mush},4\rightarrow 5} = (c_{\text{mush}} + (1 - a_w)w_{\text{mush}})\dot{m}_{\text{storm}} = w_{\text{mush}} \left( \frac{1}{f_{\text{H}_2\text{O}}} - a_w \right) \dot{m}_{\text{storm}}. \quad (4)$$

243 As previously, we account for the entrainment of air in the downdraft, with a mass  
 244 fraction of condensates  $q_{\text{down}}$ . This time, two limiting cases are  $q_{\text{down}} \sim 1$  if mushballs  
 245 do reach layer 5 before evaporating (e.g., if ventilation coefficients have been overesti-  
 246 mated – see Paper I), and  $q_{\text{down}} \sim$  otherwise. As previously, the compensating upward  
 247 flux is

$$\dot{m}_{4\rightarrow 5} = \dot{m}_{\text{mush},4\rightarrow 5}/q_{\text{down}} \equiv \varpi_{\text{down}}\dot{m}_{\text{storm}}, \quad (5)$$

248 where  $\varpi_{\text{down}} = (1 - a_w f_{\text{H}_2\text{O}}) w_{\text{mush}}/(f_{\text{H}_2\text{O}} q_{\text{down}})$ .

249 Parameters of our toy model are summarized in Table 1.

250 Let us consider as an example layer 1, of mass  $M_1$  and ammonia mixing ratio  
 251  $c_1$ . As shown in Fig. 2, small-scale convection brings per time  $\delta t$  a mass of ammonia  
 252  $c_2\dot{m}_{\text{conv}}\delta t$  and removes  $c_1\dot{m}_{\text{conv}}\delta t$ . Similarly storms deliver directly from layer 3 to  
 253 layer 1 a mass of ammonia  $c_3\dot{m}_{\text{storm}}\delta t$  and compensating subsidence removes at the  
 254 same time a mass  $c_1\dot{m}_{\text{storm}}\delta t$ . These storms also lead, through the formation of mush-  
 255 balls, to a removal of  $c_{\text{mush}}\dot{m}_{\text{storm}}\delta t$  of ammonia, which is transported directly to layer  
 256 5 and to a compensating upward mass flux of ammonia  $c_2\dot{m}_{\text{mush}}\delta t$ . Thus, the change  
 257 in ammonia mass in layer 1 is

$$\Delta c_1 M_1 = (c_2 - c_1)\dot{m}_{\text{conv}}\delta t + (c_3 - c_1 - c_{\text{mush}} + c_2\varpi_{\text{mush}})\dot{m}_{\text{storm}}\delta t.$$

258 Since we are looking for a steady-state solution, the equation governing the ammonia  
 259 mass balance for layer 1 is

$$0 = (c_2 - c_1)\dot{m}_{\text{conv}} + (c_3 - c_1 - c_{\text{mush}} + c_2\varpi_{\text{mush}})\dot{m}_{\text{storm}},$$

260 i.e. a simple equation independent of the mass of the layer itself. The same approach  
 261 can then be used for each layer. In order to close the system, we choose as limiting  
 262 condition that the mixing ratio of the bottom layer is prescribed to the value inferred  
 263 from the Juno measurement.

264 For water, with a mixing ratio  $w$ , the equations are the same, but we must  
 265 consider that water is only present in condensed form in layers 1 and 2 and will  
 266 therefore very rapidly be transported back to layer 3. Also, on the basis of Paper I,  
 267 we consider that a fraction  $a_w$  of the mushballs are evaporated in level 4 and its  
 268 counterpart  $(1 - a_w)$  in level 5. Only 3 equations are needed for level 3 and 4 and to  
 269 close the system with  $w_5 = w$ . The resulting mass balance is represented in Fig. 3.  
 270 Since layers 1 and 2 have a median abundance of water that is negligible, only 3  
 271 equations are needed for level 3 and 4 and to close the system with  $w_5 = w$ . As an  
 272 example, the mass balance equation for water in layer 3 is:

$$\Delta w_3 M_3 = (w_4 - w_3)\dot{m}_{\text{deep}}\delta t + (w_5 - w_3 - w_{\text{mush}} + w_4\varpi_{\text{down}})\dot{m}_{\text{storm}}\delta t.$$

273 As for ammonia, the steady-state solution is independent of layer mass.

274 Finally we consider in Fig. 4 energy balance in the system. Since we consider  
 275 levels at relatively high optical depth, we neglect any radiation heating/cooling. Dry  
 276 static energy,  $s \equiv c_P T + gz$  with  $c_P$  being the heat capacity of air and  $z$  altitude,  
 277 is therefore conserved during dry adiabatic motions. When condensation occurs in  
 278 updrafts or due to evaporation, moist static energy  $h = c_P T + gz + L_v w$  with  $L_v$   
 279 being the latent heat of vaporization of water, is approximately conserved (Holton,  
 280 1992). (For this simple model, we neglect the effect of the condensation of ammonia  
 281 because of its expected much smaller abundance). Equivalently, dry static energy is  
 282 increased by  $L_v w$  by the condensation of water, or decreased by the same amount  
 283 upon vaporization.

284 As illustrated by Fig. 4, dry convective events result in mixing static energy  
 285 between adjacent layers. Small-scale convection results in condensation of transported  
 286 water in layer 2 and its vaporization in layer 3, resulting in positive and negative  
 287 contributions in these respective layers. Storms lead to condensation of water and  
 288 transport of the static energy to level 1. Part of the water flux is reevaporated in  
 289 layer 3. The other part forms mushballs which reevaporate (and deliver a negative  
 290 static energy contribution) in layers 4 and 5. Note that in this simple model, we do  
 291 not consider the small contribution of water (or ammonia) gases to the static energy  
 292 budget and we also neglect any possible condensation events linked to the small upward  
 293 mass flux that balances the downward flux of mushballs.

294 As an example, for layer 2, we must consider the advection of static energy to  
 295 and from adjacent layers, and we have to include a term due to the release of latent

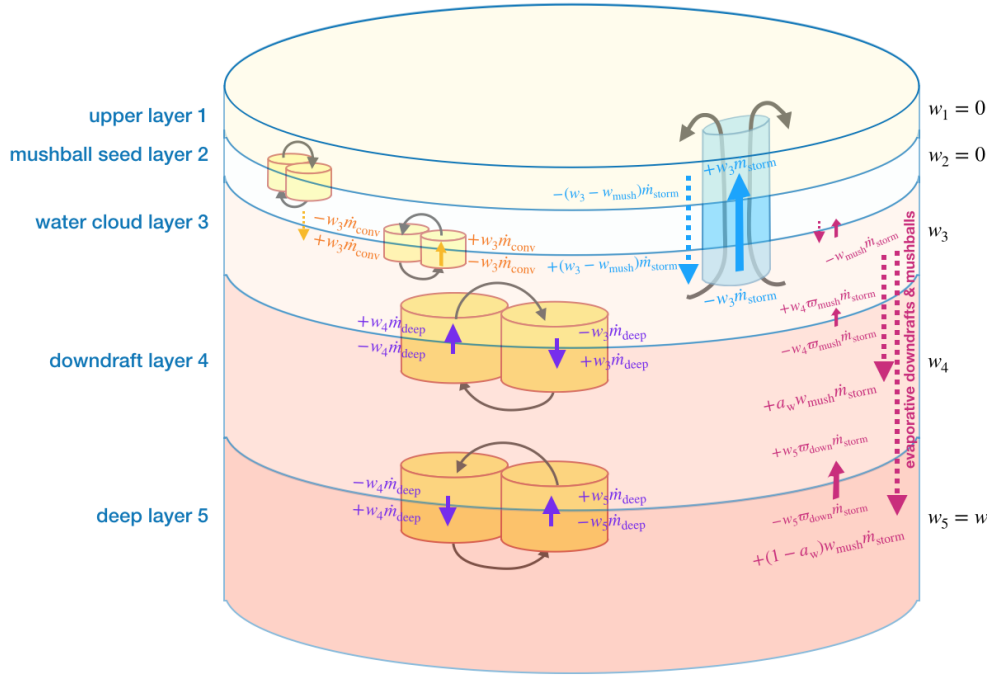


**Figure 3.** As Fig. 2 for the mass balance of water in the framework of our 5-layer model.

296 heat due to water condensation during small-scale convection events. Thus,

$$\Delta s_2 M_2 = (s_3 + s_1 - 2s_2 + w_3 L_{\text{H}_2\text{O}}) \dot{m}_{\text{conv}} \delta t + (s_1 - s_2) \dot{m}_{\text{storm}} \delta t.$$

297 For layer 5, we have to consider the internal heat flux  $F_{\text{tot}} \delta t$ . Accounting for the  
 298 evaporation of mushballs and static energy transport the energy budget for that layer  
 299 is:

$$\Delta s_5 M_5 = (s_4 - s_5) \dot{m}_{\text{conv}} \delta t + [-(1 - a_w) w_{\text{mush}} L_v - s_5 \varpi_{\text{deep}}] \dot{m}_{\text{storm}} \delta t + F_{\text{tot}} \delta t.$$

300 Overall, because we are looking for a steady-state solution, the solution is indepen-  
 301 dent of the value of the mass flux itself. It is convenient to define

$$\begin{cases} f_{\text{conv}} \equiv \dot{m}_{\text{conv}} / \dot{m}_{\text{deep}} \\ f_{\text{storm}} \equiv \dot{m}_{\text{storm}} / \dot{m}_{\text{deep}} \end{cases} \quad (6)$$

302 We can thus obtain 5 equations for the ammonia mass balance, 3 for the water mass  
 303 balance and 5 for the energy balance (including the 3 boundary conditions), as follows:

$$\begin{cases} (c_2 - c_1) f_{\text{conv}} + [c_3 - c_1 - c_{\text{mush}} + c_2 \varpi_{\text{mush}}] f_{\text{storm}} = 0, \\ (c_3 + c_1 - 2c_2) f_{\text{conv}} + [c_1 - c_2 + (c_3 - c_2) \varpi_{\text{mush}}] f_{\text{storm}} = 0, \\ (c_4 - c_3) + (c_2 - c_3) f_{\text{conv}} + [c_2 - c_3 + (c_4 - c_3) \varpi_{\text{mush}}] f_{\text{storm}} = 0, \\ (c_5 + c_3 - 2c_4) + [c_5 \varpi_{\text{down}} - c_4 \varpi_{\text{mush}}] f_{\text{storm}} = 0, \\ c_5 = c, \\ (w_4 - w_3) + [-w_{\text{mush}} + w_4 \varpi_{\text{mush}}] f_{\text{storm}} = 0 \\ (w_5 + w_3 - 2w_4) + [a_w w_{\text{mush}} + w_5 \varpi_{\text{down}} - w_4 \varpi_{\text{mush}}] f_{\text{storm}} = 0, \\ w_5 = w, \\ s_1 = s_0, \\ (s_3 + s_1 - 2s_2 + w_3 L_v) f_{\text{conv}} + [s_1 - s_2 + (s_3 - s_2) \varpi_{\text{mush}}] f_{\text{storm}} = 0, \\ (s_4 - s_3) + (s_2 - s_3 - w_3 L_v) f_{\text{conv}} + [s_2 - s_3 - (w_3 - w_{\text{mush}}) L_v + (s_4 - s_3) \varpi_{\text{mush}}] f_{\text{storm}} = 0, \\ (s_5 + s_3 - 2s_4) + [-a_w w_{\text{mush}} L_v + s_5 \varpi_{\text{down}} - s_4 \varpi_{\text{mush}}] f_{\text{storm}} = 0, \\ (s_4 - s_5) + [-(1 - a_w) w_{\text{mush}} L_v - s_5 \varpi_{\text{down}}] f_{\text{storm}} + F_{\text{tot}} / \dot{m}_{\text{deep}} = 0. \end{cases} \quad (7)$$

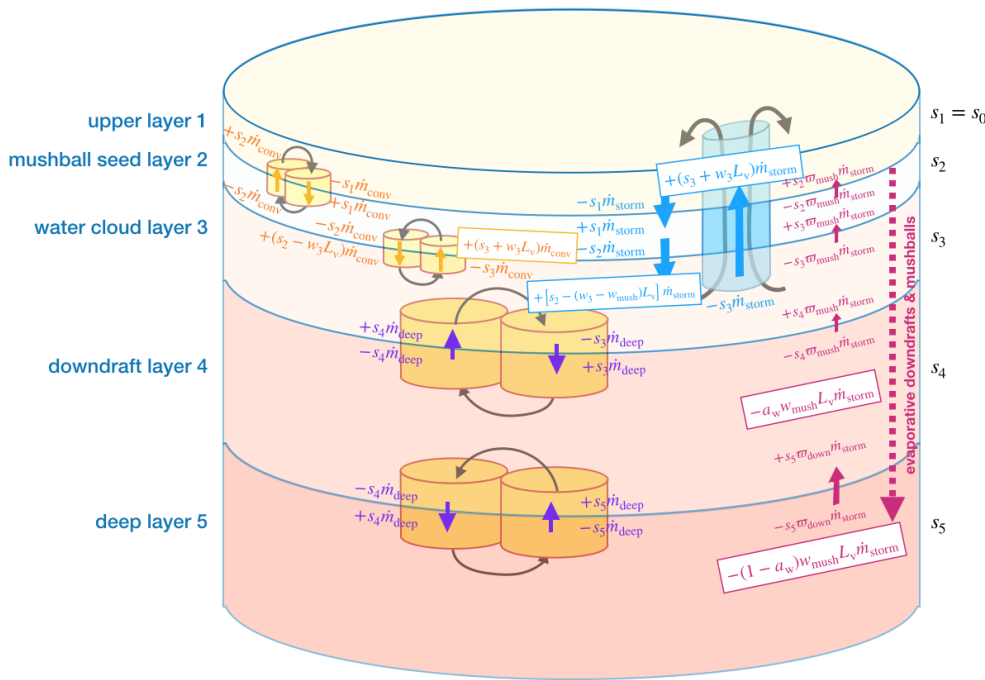


**Figure 4.** As Fig. 2 for the balance of static energy in the framework of our 5-layer model. In addition to the terms due to a transport of static energy, terms resulting from the condensation or evaporation of water are highlighted.

304 **3.2 Static energy and potential temperature**

305 Instead of static energy, it is generally convenient to express the results in terms  
 306 of potential temperature

$$\theta \equiv T(P/P_0)^{-\mathcal{R}/c_P}, \tag{8}$$

307 For a dry atmosphere and a perfect gas, the potential temperature defined by Eq. (8)  
 308 by is directly linked to the entropy. For a real atmosphere, the changes in specific  
 309 heat, mean molecular weight and the departures from an ideal gas are thought of  
 310 being relatively small (at the percent level), so that the potential temperature at deep  
 311 levels can be used as a useful estimate of the boundary condition that should be  
 312 used for interior models. Current interior models are generally based on the Voyager  
 313 measurements of  $165 \pm 5$  K at 1 bar (Lindal, 1992; Guillot, 2005). The Galileo probe  
 314 measured a temperature at 1 bar of  $166.1 \pm 0.2$  K (Seiff et al., 1998). For a dry adiabatic  
 315 atmosphere, we would thus expect that at deep levels in Jupiter  $\theta \approx 166$  K. However  
 316 the Galileo probe measured a temperature at 22 bar of  $427.7 \pm 1.5$  K (Seiff et al., 1998),  
 317 about 4 K colder than expected for a dry adiabat (Leconte et al., 2017). Assuming  
 318  $\mathcal{R}/c_P \sim 0.3$ , this implies a change in potential temperature  $\Delta\theta \sim -1.6$  K.

319 In order to link the deviations in static energy to those in potential temperature  
 320 in our simple model, we use the fact that  $ds = c_P dT + gdz = c_P T d\theta/\theta$ . Using Eq. 8,  
 321 this implies

$$d\theta = \left(\frac{P}{P_0}\right)^{-\mathcal{R}/c_P} \frac{ds}{c_P}, \tag{9}$$

322 i.e. the deviations of the potential temperature at each level can be obtained by  
 323 integrating changes in the static energy at each level.

324 We thus derive the potential temperature difference at 1 bar as  $\Delta\theta_i = \theta_i - \theta_1$   
 325 based on the static energies for each level calculated from Eq. 7, the pressure levels  
 326 defined in Section 2 and  $\mathcal{R}/c_P = 0.3$ .

### 327 3.3 Solutions as a function of $f_{\text{storm}}$

328 We now examine the solutions of Eq. 7 as a function of our  $f_{\text{storm}}$  parameter for  
 329 our fiducial parameters (see Table 1). Figure 5 shows the resulting mixing ratios of  
 330  $\text{H}_2\text{O}$  and  $\text{NH}_3$  and the potential-temperature anomalies for the 5 layers considered.  
 331 For convenience, we plot the solutions in terms of the volume mixing ratios, calculated  
 332 with the approximate relations  $x_{\text{NH}_3} \approx (\mu/\mu_{\text{NH}_3})c$  and  $x_{\text{H}_2\text{O}} \approx (\mu/\mu_{\text{H}_2\text{O}})w$ .

333 The two columns of Fig. 5 correspond to two different situations. The left col-  
 334 umn corresponds to a case in which storms carry most of the internal heat in the  
 335 water condensation region, a situation that is relevant to the mid-latitudes in Jupiter  
 336 (Gierasch et al., 2000). The minimum  $\text{NH}_3$  concentration is obtained for large values  
 337 of  $f_{\text{storm}}$ . The Juno MWR observations of a 100 to 250 ppmv ammonia abundance  
 338 thus indicate that, at mid-latitudes,  $f_{\text{storm}} \geq 1$  (for  $\epsilon = 0.3$ ). On the contrary, the  
 339 Equatorial Zone, represented by the right column of Fig. 5 is characterized by a rel-  
 340 atively uniform ammonia abundance and thus requires  $f_{\text{storm}} \leq 0.2$ , in line with the  
 341 lack of storms and lightning there.

342 We can thus explain a low abundance of ammonia to great depth if (1) strong  
 343 storms are able to loft water ice particles into the mushball-formation region and (2)  
 344 they occur more frequently than material is mixed upward in deep regions of Jupiter.  
 345 This is a situation that appears to occur in most regions of Jupiter. In the Equatorial  
 346 Zone these two conditions appear not to be fulfilled, explaining the high and relatively  
 347 vertically uniform abundance of ammonia there.

348 The temperature structure that can be inferred from Fig. 5 is characterized by  
 349 a standard moist adiabatic profile in the Equatorial Zone and an extended moist  
 350 adiabat driven by the evaporation of mushballs at mid-latitudes. Superadiabaticity  
 351 factors may also play a role: while for Fig. 5 we assumed that  $F_{\text{tot}}/\dot{m} \ll wL_v$ , it may  
 352 not be the case. In fact, in order to explain values  $f_{\text{storm}} > 1$ , the superadiabaticity  
 353 at deep levels  $\delta\theta_{\text{deep}}$  should be larger than in the water condensation region  $\delta\theta_{\text{storm}}$ ,  
 354 since in the absence of significant radiative transport, energy balance requires that  
 355  $\dot{m}c_P\delta\theta_{\text{deep}} \sim f_{\text{storm}}\dot{m}c_P\delta\theta_{\text{storm}}$ . This could lead to significant modifications of the  
 356 interior adiabat and deserves detailed studies.

### 357 3.4 Analytical solutions

358 The system of equations defined by Eq. 7 may be solved analytically with a  
 359 few simplifications. First, we neglect the return upward flow arising from the fall of  
 360 mushballs and evaporative downdrafts. This is justified as long as little atmospheric  
 361 gas is entrained with mushballs and downdrafts (i.e.,  $\varpi_{\text{mush}} \ll w_{\text{mush}}/w$  and  $\varpi_{\text{down}} \ll$   
 362  $w_{\text{mush}}/w$ ). We then assume that water is abundant so that the mushball production is  
 363 always limited by the availability of ammonia, i.e. that  $w_3 > (c_2 - c_{\text{min}})f_{\text{H}_2\text{O}}/f_{\text{NH}_3}$ .  
 364 Finally, we ignore small-scale convection in the upper atmosphere ( $f_{\text{conv}} = 0$ ). In that

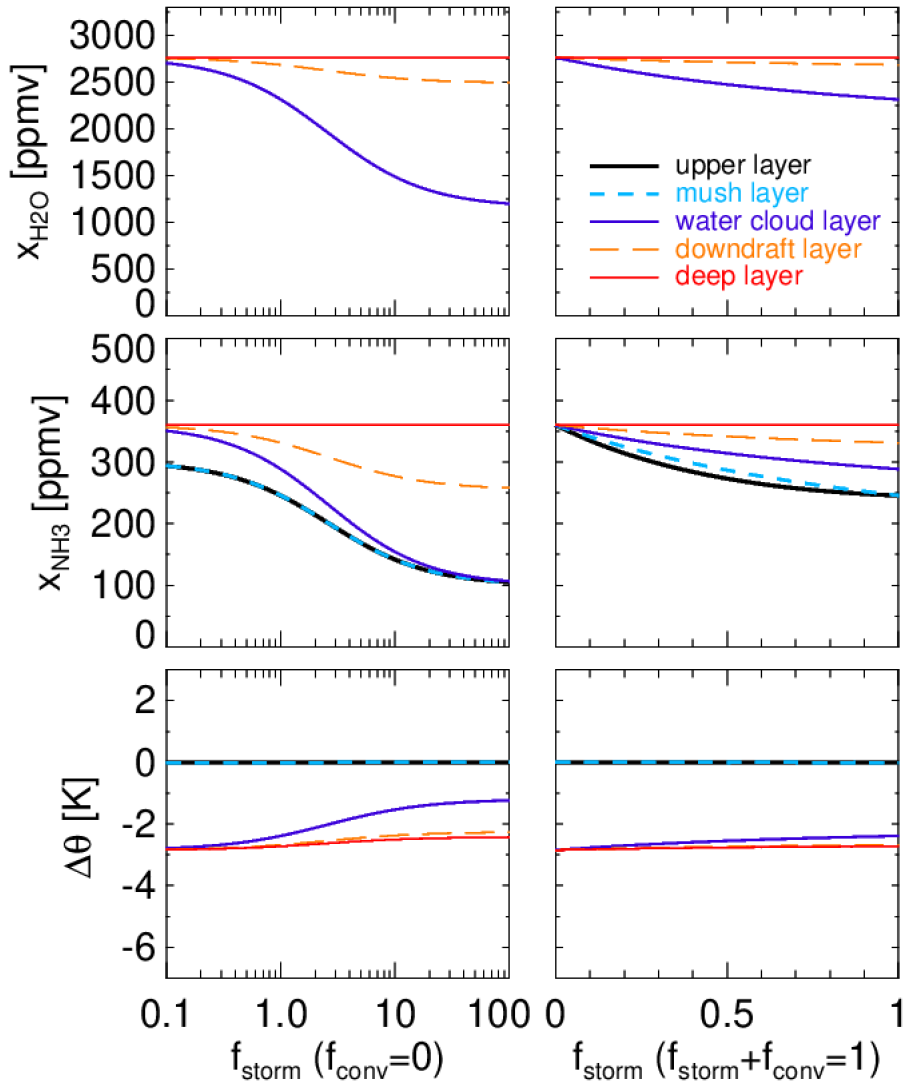


**Figure 5.** Abundances of water (top row), ammonia (middle row) and potential-temperature anomalies (bottom row) obtained with our model, as a function of  $f_{\text{storm}}$ , a parameter assessing the mass flux in large water storms relative to that of dry convection below the water cloud base. The left column corresponds to a situation in which no small-scale convection is present in the water condensation region ( $f_{\text{conv}} = 0$ ) and pertains to mid-latitude regions of Jupiter. The right column assumes that both small-scale convection and storms occur, so that  $f_{\text{storm}} + f_{\text{conv}} = 1$ . The curves show the different layers considered in Fig. 5: 1) upper layer (purple); 2) mushball-seed layer (blue, dashed); 3) water cloud layer (light blue); 4) downdraft layer (orange, dashed); 5) deep (red). The potential-temperature anomalies are calculated assuming that intrinsic heat flux transport occurs with negligible superadiabaticity (see text).

365 case the system of equations yields:

$$\left\{ \begin{array}{l}
 c_1 = c_2 = c_{\min} + \frac{c - c_{\min}}{1 + \epsilon + 2\epsilon f_{\text{storm}}} \\
 c_3 = c_{\min} + \frac{(c - c_{\min})(1 + \epsilon)}{1 + \epsilon + 2\epsilon f_{\text{storm}}} \\
 c_4 = \frac{c(1 + \epsilon + \epsilon f_{\text{storm}}) + c_{\min}\epsilon f_{\text{storm}}}{1 + \epsilon + 2\epsilon f_{\text{storm}}} \\
 w_3 = w - (2 - a) \frac{(c - c_{\min})(f_{\text{H}_2\text{O}}/f_{\text{NH}_3}) \epsilon f_{\text{storm}}}{1 + \epsilon + 2\epsilon f_{\text{storm}}} \\
 w_4 = w - (1 - a) \frac{(c - c_{\min})(f_{\text{H}_2\text{O}}/f_{\text{NH}_3}) \epsilon f_{\text{storm}}}{1 + \epsilon + 2\epsilon f_{\text{storm}}} \\
 s_1 = s_2 = s_0 \\
 s_3 = s_0 - L_v w_3 + \frac{F_{\text{tot}}}{\dot{m} f_{\text{storm}}} \\
 s_4 = s_0 - L_v w_4 + \frac{F_{\text{tot}}(1 + f_{\text{storm}})}{\dot{m} f_{\text{storm}}} \\
 s_5 = s_0 - L_v w + \frac{F_{\text{tot}}(2 + f_{\text{storm}})}{\dot{m} f_{\text{storm}}}
 \end{array} \right. \quad (10)$$

366 Thus when  $\epsilon f_{\text{storm}} \gg 1$ ,  $c_1 = c_2 = c_3 \approx c_{\min}$ ,  $c_4 \approx (c + c_{\min})/2$  and  $w_3 \approx$   
 367  $w - (1 - a/2)(c - c_{\min})(f_{\text{H}_2\text{O}}/f_{\text{NH}_3})$ ,  $w_4 \approx w - (1/2 - a/2)(c - c_{\min})(f_{\text{H}_2\text{O}}/f_{\text{NH}_3})$ .  
 368 When storms dominate the mass transport over the deep convection, the atmosphere  
 369 is depleted in ammonia all the way to the deepest layer. The water abundance in  
 370 layers 3 and 4 is controlled by the parameter  $f_{\text{H}_2\text{O}}/f_{\text{NH}_3}$ , i.e., by the ratio of water  
 371 to ammonia in mushballs. This parameter crucially depends on the microphysics of  
 372 particle growth and is thus very difficult to estimate, implying that we cannot at this  
 373 point provide a quantitative estimate of the abundance of water. Importantly, in that  
 374 limit, the process is independent of  $\epsilon$ , the efficiency of mushball formation.

375 The conditions for the mushball mechanism to deplete the deep atmosphere in  
 376 ammonia can be derived from our analytical relations in the limit of negligible small-  
 377 scale convection. A first condition is that mushball production should be limited  
 378 by the availability of ammonia rather than water. This occurs when  $f_{\text{NH}_3}/f_{\text{H}_2\text{O}} >$   
 379  $(c - c_{\min})/w$  (implying  $f_{\text{NH}_3} \gtrsim 0.09$  for a solar deep N/O ratio). The second condition  
 380 is that  $f_{\text{storm}} \gtrsim 1/\epsilon$ . Thus, even an inefficient mushball formation mechanism can lead  
 381 to a depletion of ammonia to great depth, as long as storms are much more frequent  
 382 than updrafts in the deep atmosphere, below the water cloud base.

383 Since we are neglecting radiative heating and cooling, static energy is uniform in  
 384 layers 1 and 2, a consequence of dry adiabatic motions by compensating subsidence. In  
 385 the layers below, static energy decreases due to the evaporation of water ice and rain:  
 386 the temperature gradient becomes smaller than a dry adiabat, and in fact equivalent  
 387 to a moist adiabat. However it is important to note that this change extends even  
 388 deeper than the water cloud base because of the sinking of mushballs to great depth.

389 With these solutions, we can relate ammonia abundances (as found from MWR)  
 390 to the value of the  $f_{\text{storm}}$  parameter. In order to consider both the equatorial region  
 391 and the other latitudes, this time, we assume  $f_{\text{conv}} = 1$ . The relation between  $f_{\text{storm}}$   
 392 and  $c_3$  is:

$$f_{\text{storm}} = \frac{c + c\epsilon - c_3 - 3\epsilon c_3 + 2\epsilon c_{\min} + \sqrt{8\epsilon(c - c_3)(c_3 - c_{\min}) + (c + c\epsilon - (1 + 3\epsilon)c_3 + 2\epsilon c_{\min})^2}}{4\epsilon(c_3 - c_{\min})} \quad (11)$$

393 This relation assumes  $f_{\text{conv}} = 1$ , an approximation that allows to consider the equator  
 394 and mid-latitude regions with the same model.

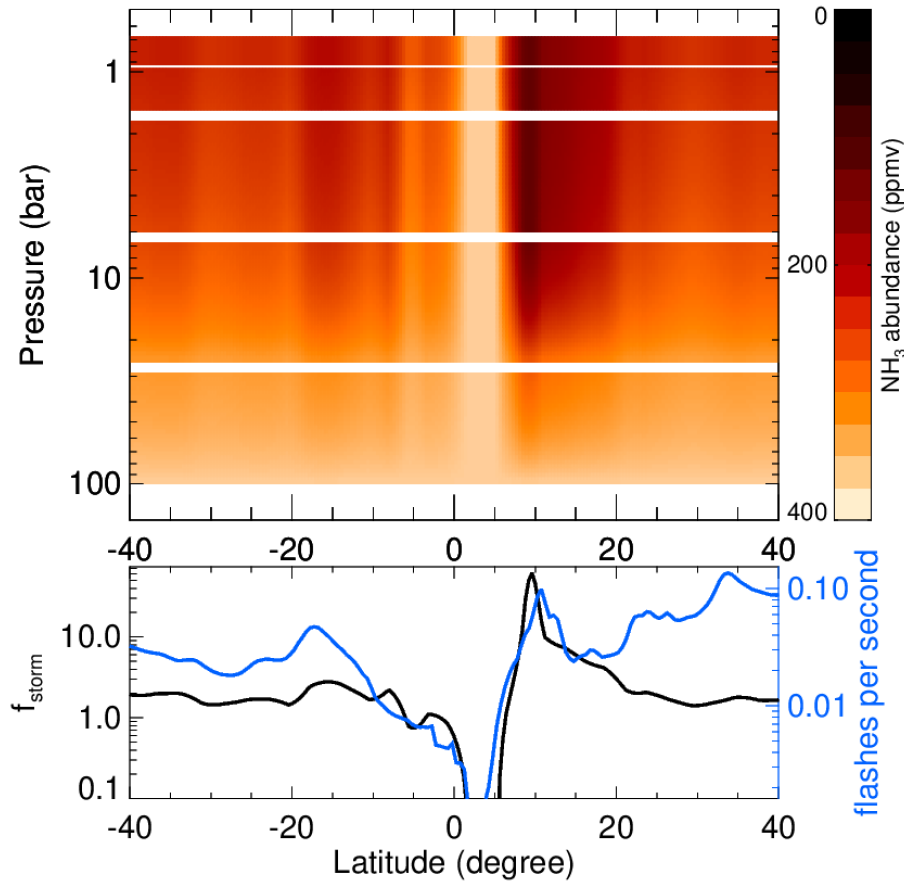


**Figure 6.** Distribution of ammonia concentration obtained with our conceptual model. The top panel shows the  $\text{NH}_3$  mixing ratio as a function of latitude and pressure in the 5 layers of our model. The bottom panel indicates the value of  $f_{\text{storm}}$  (black line) obtained to reproduce the 1-3 bar MWR ammonia mixing ratio compared to the number of flashes per second detected by the MWR instrument between PJ1 and PJ16 (Brown et al., 2018). The large and uniform ammonia concentration in the Equatorial Zone is well reproduced by assuming a scarcity of storms ( $f_{\text{storm}} \sim 0$ ), in line with the absence of lightning there. At mid-latitudes, frequent storms and subsequent mushball formation lead to a depletion in ammonia.

## 395 4 Application to the MWR Juno results

### 396 4.1 Reproducing the MWR Juno measurements

397 We now compare the MWR ammonia abundance-latitude map to our theoretical  
 398 model. In order to estimate the value of  $f_{\text{storm}}$  per latitude, we use Eq. (11) with the  
 399 ammonia abundance from MWR (see Fig. 1) in the 1-3 bar region. We then use this  
 400 value in our full model defined by Eq. (7) and our fiducial parameters from Table 1.  
 401 We interpolate linearly the values of the mixing ratios as a function of depth (in  $\log P$ )  
 402 to produce a map of the ammonia mixing ratios as a function of latitude and depth.

403 The results are presented in Figure 6. The dominant features, i.e., the nearly  
 404 uniform abundance of ammonia in the Equatorial Zone and its depletion elsewhere  
 405 are explained by a change of the nature of convection at these latitudes, from being  
 406 mostly small-scale (vertically) at the equator to being large-scale and dominated by

407 water storms elsewhere. While our simple model is insufficient to explain the details  
 408 of the ammonia distribution in the deep atmosphere, the suppression of storms at the  
 409 equator is fully consistent with the Juno observation of a lack of lightning events at  
 410 the equator (Brown et al., 2018), with the value of  $f_{\text{storm}}$  showing a clear correlation  
 411 to the MWR lightning rate there (Fig 6, bottom panel). The reason for the absence  
 412 of storms itself, however, is not clear. It could be that vertical shear is absent in  
 413 the Equatorial Zone and that the formation of rain and subsequent mass loading of  
 414 water storms prevents their ascent (Rafkin & Barth, 2015). At the other extreme, it  
 415 could also be that the Equatorial Zone experiences a very strong vertical shear that  
 416 effectively extinguishes storm formation. Insolation, which is strongest at the equator,  
 417 is also an important factor to consider.

## 418 4.2 Ammonia and water

419 The depletion of ammonia to great depths measured by Juno MWR is reminiscent  
 420 of a long-standing issue, that of Jupiter’s deep water abundance. Already in the  
 421 1980s, 5- $\mu\text{m}$  spectroscopic observations of Jupiter’s atmosphere had revealed a very  
 422 low abundance of water vapor, one to two orders of magnitude less than the solar  
 423 value, down to at least 6 bars in a wide region covering  $-40^\circ$  to  $+40^\circ$  latitude, with  
 424 three times lower abundance in Jupiter’s hot spots (Bjoraker et al., 1986). A simple  
 425 explanation was proposed: Jupiter’s water clouds form narrow columns of humid air  
 426 inside which water efficiently rains out to the cloud base, leaving the remaining region  
 427 dry because of compensating subsidence (Lunine & Hunten, 1987). However this simple  
 428 idea was shown to be incompatible with an Earth-based parametrization of cumulus  
 429 clouds (del Genio & McGrattan, 1990), for at least two reasons. First, compensating  
 430 subsidence stabilizes the atmosphere and prevents further cumulus cloud activity, and  
 431 second, upward mixing tends to bring moisture up from the cloud base level which is  
 432 itself soaked by rain reevaporation. The picture, further strengthened by later detailed  
 433 microphysical models (Palotai & Dowling, 2008), held to this day. When the Galileo  
 434 probe measured an extremely low abundance of water in a 5- $\mu\text{m}$  hot spot (Niemann  
 435 et al., 1998; Wong et al., 2004), the explanation was that this was a special region of  
 436 Jupiter, mostly downwelling and consequently dry, due to global-scale wave activity  
 437 (Ortiz et al., 1998; Showman & Ingersoll, 1998; Showman & Dowling, 2000; Friedson,  
 438 2005).

439 Yet, to this day, Jupiter’s atmospheric water and ammonia abundances retrieved  
 440 from spectroscopic observation remain incompatible with predictions of cloud models  
 441 and global circulation models. The analysis of Galileo/NIMS and Juno/JIRAM spec-  
 442 troscopic observations (Roos-Serote et al., 2004; Grassi et al., 2017, 2020) essentially  
 443 confirm the previous observations by Bjoraker et al. (1986). In order to reproduce  
 444 the 5- $\mu\text{m}$  spectra in the North Equatorial Belt, one generally requires a very low  
 445 water abundance to great depths (8 bars or so), or at least a low relative humidity  
 446 ( $\sim 10\%$ ) until a cloud deck with a high opacity is reached. In addition, even though  
 447 wave activity can explain qualitatively the low water abundance in 5- $\mu\text{m}$  hot spots,  
 448 the fact that the depletion persists down to at least 22 bars as measured by the Galileo  
 449 probe remains unaccounted for.

450 Our model accounts for a low ammonia abundance in region where storms are  
 451 frequent. Because the fate of water is tied to that of ammonia, as shown in Fig. 5, water  
 452 is expected to be depleted as well. This could thus potentially explain the observations  
 453 of both ammonia and water in Jupiter. The fact that this was not identified in previous  
 454 studies is tied to three factors: (i) Hail is a very rare process on Earth and had always  
 455 been neglected in studies of Jupiter’s storms and general-circulation models. As shown  
 456 in Paper I, the presence of a region where a liquid  $\text{NH}_3 \cdot \text{H}_2\text{O}$  mixture is bound to form  
 457 is a pathway to hail formation. Such a property had not been identified previously,  
 458 and thus hail formation was not considered in microphysical models (Yair et al., 1995;

459 Palotai & Dowling, 2008; Sugiyama et al., 2014; C. Li & Chen, 2019). (ii) Evaporative  
 460 downdrafts have small-scales and are notoriously difficult to model. As shown in  
 461 Paper I, they can efficiently transport a heavy condensable species even through layers  
 462 where equilibrium chemistry would predict a complete mixing. (iii) Vertical diffusion  
 463 by other processes was assumed to be more important than small-scale transport.

### 464 4.3 Consequences for Jupiter’s deep atmospheric structure

465 Our model is bound to have strong consequences for Jupiter’s deep atmospheric  
 466 structure, in relation to its deeper internal structure. The molecular weight increase  
 467 below the water condensation level due to the increase in both ammonia and water  
 468 abundance, is estimated to be of order  $\Delta\mu/\mu \sim 10^{-2}$ . (This is an order-of-magnitude  
 469 value based on Fig. 5, with our hypothesis of a solar N/O ratio). Because this takes  
 470 place in a region where condensation is not possible, convection will be suppressed  
 471 by this molecular weight gradient except where temperature fluctuations (or the tem-  
 472 perature increase over a dry adiabat) is of order  $\Delta T_\mu/T \sim \Delta\mu/\mu$ , corresponding to a  
 473 3 K temperature increase at 300 K. What seems like a tiny increase is in fact highly  
 474 significant as can be seen from two quantities.

475 First, let us introduce the convective available potential energy (CAPE) in the  
 476 water-condensation region, which measures the ability of storms to develop and be  
 477 extremely significant. The maximum value of this quantity can be calculated by as-  
 478 suming that the atmosphere follows a dry adiabat in the water-condensation region  
 479 and that the humidity is 100% at cloud base. In that case, the maximum energy  
 480 released is approximately

$$\text{CAPE}_{\text{Max}} = x_{\text{H}_2\text{O}}(\mu_{\text{H}_2\text{O}}/\mu)L_{\text{H}_2\text{O}} \approx 46 \times 10^7 \text{ erg/g}, \quad (12)$$

481 for our fiducial water abundance (this value is of course proportional to the water  
 482 abundance). Of course, this base temperature profile is violently unstable so that  
 483 we expect in real situation much smaller values arising from an temperature gradient  
 484 in the atmosphere that is close to a moist adiabat. On Earth, this value is similar  
 485 (the mean molecular weight of the atmosphere is one order of magnitude higher, but  
 486 300 K is reached near 1 bar rather than near 6 bar in Jupiter, implying that the water  
 487 volume mixing ratio is about 6 times larger on Earth), but in fact the most violent  
 488 thunderstorms generally associated with hail formation in the Earth atmosphere occur  
 489 when the value of CAPE reaches only about  $5 \times 10^7 \text{ erg/g}$ .

490 Now, in Jupiter, the increased temperature needed for a convective perturbation  
 491 to bypass the molecular weight gradient is equivalent to an added CAPE

$$\Delta\text{CAPE}_\mu = c_{P, \text{atm}}\Delta T_\mu \approx 85 \times 10^7 \text{ erg/g}, \quad (13)$$

492 where we used  $c_{P, \text{atm}} = 28 \times 10^7 \text{ erg/(gK)}$  (see Paper I) and as above  $\Delta T_\mu \approx 3 \text{ K}$ .  
 493 Thus deep convective events can potentially power extremely violent storms on Jupiter.  
 494 Whether this is actually the case will depend on other processes, such as the balance  
 495 between cooling by downdrafts and heating by convection from deeper regions.

496 Another aspect to consider is the superadiabatic gradient needed to overcome the  
 497 molecular weight gradient, i.e.,  $\nabla_{s, \text{ad}} \equiv (d \ln T / d \ln P) - (\partial \ln T / \partial \ln P)_S \approx \Delta T_\mu / T / \Delta \ln P$ ,  
 498 where  $\Delta \ln P$  corresponds to the extent of the inhomogeneous region. Even if we con-  
 499 sider that the region is extremely extended (say  $\Delta \ln P = 10$ ), this would imply a  
 500 superadiabatic gradient  $\nabla_{s, \text{ad}} \gtrsim 10^{-3}$ . In general, mixing length theory predicts that  
 501 the superadiabatic gradient should be much smaller, i.e.,  $\nabla_{s, \text{ad}} \lesssim 10^{-5}$  (Guillot et al.,  
 502 2004). This implies that convective events are transporting much more energy at a  
 503 time and therefore should be much less frequent. Equivalently, this implies that the  
 504  $\dot{m}_{\text{deep}}$  parameter should be small, justifying a posteriori our finding that  $f_{\text{storm}}$  can be  
 505 significantly larger than unity.

506 Finally, it is important to note that evaporative downdrafts are delivering cool  
 507 air to the deep atmosphere, providing another pathway to transport the internal heat  
 508 from the deep region. This can potentially suppress convection at depth, in the down-  
 509 draft region. For this to occur, the mushball flux needs to be such that the evaporative  
 510 cooling balances the internal heating, i.e.,  $\dot{m}_{\text{mush}} = F_{\text{tot}}/L_v \approx 3 \times 10^{-7} \text{ g}/(\text{cm}^2 \text{ s})$ . In  
 511 Jupiter, the number of storms per area is variable, but for example in the north equato-  
 512 rial belt it reaches  $N_{\text{storms}} \sim 2 \times 10^{-9} \text{ km}^{-2}$  (Brown et al., 2018). This implies that to  
 513 offset convection at depth, each storm should dump  $(F_{\text{tot}}/L_v)/N_{\text{storms}} \sim 1.5 \times 10^{12} \text{ g/s}$   
 514 of condensates (mushballs). Assuming a typical storm area  $\sigma_{\text{storm}} \sim 300 \text{ km} \times 300 \text{ km}$ ,  
 515 we can calculate that the precipitation rate should be  $F_{\text{tot}}/(L_v N_{\text{storms}} \tilde{\rho} \sigma_{\text{storm}}) \sim$   
 516  $6 \text{ cm/hr}$ . On Earth, this would be classified as violent precipitation (in the form of  
 517 rain, generally). With larger storm areas, an even weaker precipitation rate can offset  
 518 heating by the planet’s internal heat flux.

519 This precipitation rate is significantly smaller than the maximum precipitation  
 520 rate on Jupiter, obtained from  $w \rho_{\text{cloud base}} v_{\text{updraft}}/\tilde{\rho} \sim 220 \text{ cm/hr}$ . (We have assumed  
 521  $w \sim 0.02$ ,  $\rho_{\text{cloud base}} \sim 5 \times 10^{-3} \text{ g/cm}^3$ ,  $v_{\text{updraft}} = 50 \text{ m/s}$ ). So even with an efficiency  
 522 of 3%, strong storms in Jupiter may suppress convection at depth, providing a self-  
 523 consistent explanation for the high  $f_{\text{storm}}$  values that we obtain at some latitudes.

#### 524 4.4 Caveats

525 Of course, some important caveats must be added. We have neglected three  
 526 crucial ingredients that eventually must be included: (i) large-scale advection and  
 527 diffusion processes, (ii) radiative heating/cooling, and (iii) rotation.

528 In our model, the ammonia (and water) transported downward by mushballs and  
 529 evaporative downdrafts are only carried upward again by compensating subsidence. In  
 530 the limit  $f_{\text{storm}} \gg 1$ , this represents an absolute minimum to the amount of vertical  
 531 transport and allows vertical abundance gradients to develop. Of course, observations  
 532 of anticyclones and the relative success in modeling them (García-Melendo et al., 2009;  
 533 Palotai et al., 2014) show that global-scale circulation matters. The MWR map from  
 534 Fig. 1 show some structures that are not matched by our simple model in Fig. 6. In  
 535 reality, both small-scale storms and large-scale circulation must play a role and shape  
 536 the vortices that we see everywhere in Jupiter’s atmosphere.

537 We have neglected radiative heating/cooling, and the frequency of storms that  
 538 we infer is not self-consistently calculated as a function of stability arguments. We  
 539 thus have not proven that we can self-consistently obtain high values of  $f_{\text{storm}}$  while  
 540 transporting Jupiter’s heat flux. This will require dedicated calculations including  
 541 small-scale features such individual storms and large-scale structures with radiative  
 542 transfer. The fact that the solar heating is strongly latitude-dependent yet measured  
 543 atmospheric temperatures are nearly uniform (Ingersoll & Porco, 1978) will have to  
 544 be accounted for.

545 Our model does not include rotation, which is certainly crucial to understanding  
 546 the particularities of Jupiter’s Equatorial Zone, i.e., the absence of strong storms and  
 547 relative vertical uniformity of its ammonia abundance. We propose that the lack of  
 548 storms at the equator may be related to shear, but a quantified, predictive explanation  
 549 is still lacking.

550 Finally, with only 5 layers, our model is extremely simplified and ignores im-  
 551 portant details. Our treatment of mixing small-scale convection imposes an arbitrary  
 552 length-scale, i.e., the depth of each layer, when this should be treated as a diffusion  
 553 equation with the proper parameters. The values of the  $f_{\text{storm}}$  parameter that we  
 554 calculate are therefore only indicative and should not be used to quantify the strength  
 555 of deep convection. We do not have enough resolution to distinguish between small

556 water storms (which do not reach the 1.5-bar level) and large ones, implying that  
 557 small water storms are treated as small-scale convection. This should not affect our  
 558 results except quantitatively. We do not include other species, such as  $\text{NH}_4\text{SH}$ , which  
 559 condenses around 2 bars and could sequester some of the nitrogen. Again, this should  
 560 be marginal, owing to the small abundance of sulfur with respect to nitrogen in a  
 561 solar-composition mix (i.e.  $\text{S/N}=0.19$  according to Lodders (2003)).

## 562 5 Conclusions

563 We have shown that the variability of ammonia abundance in Jupiter retrieved by  
 564 the Juno spacecraft (Bolton et al., 2017; C. Li et al., 2017) can be linked to the presence  
 565 of storms powered by water condensation. In paper I, we showed that powerful storms  
 566 could deliver water ice particles to the 1.1-1.5 bar region where they would interact  
 567 to form a liquid  $\text{NH}_3 \cdot \text{H}_2\text{O}$  mixture that would lead to the formation of mushballs  
 568 and evaporative downdrafts, potentially transporting ammonia to great depth. In the  
 569 present paper, we developed a local model of Jupiter’s deep atmosphere solving mass  
 570 and energy balance to determine whether and in which conditions we could explain  
 571 the Juno observations.

572 Our model can account at least qualitatively for the observed vertical and lat-  
 573 tudinal structure of the ammonia abundance in Jupiter. Storms powered by water  
 574 condensation lead to the formation of mushballs and evaporative downdrafts and thus  
 575 deplete the atmosphere of its ammonia and water locally. We introduced a parameter  
 576  $f_{\text{storm}}$ , the ratio of the mass transported in these water storms to the mass transported  
 577 by dry convection at greater depth, which measures the efficiency of the process. When  
 578  $f_{\text{storm}} \lesssim 1$ , the process is inefficient and the ammonia abundance remains high. This  
 579 is the situation corresponding to Jupiter’s Equatorial Zone which is characterized by  
 580 a high ammonia abundance (C. Li et al., 2017) and an absence of lightning flashes  
 581 (Brown et al., 2018). When  $f_{\text{storm}} \gg 1$ , storms are dominating the mass transport,  
 582 ammonia (and water) can be transported to great depth which explains the low mix-  
 583 ing ratio of ammonia observed at all latitudes away from the  $0^\circ - 5^\circ\text{N}$  region. When  
 584 estimating the value of  $f_{\text{storm}}$  needed to reproduce the Juno ammonia measurements,  
 585 we find that they are correlated to the flash rates measured by MWR, at least in the  
 586  $-10^\circ$  to  $10^\circ$  latitude range. Also, we find that at all latitudes, local maxima in  $f_{\text{storm}}$   
 587 correspond to local maxima of the flash rate.

588 Importantly, the efficiency of the process results from a balance between the  
 589 efficiency of mushball formation  $\epsilon$  and the value of  $f_{\text{storm}}$ . A low efficiency of mushball  
 590 formation ( $\epsilon \ll 1$ ) can lead to a significant depletion of ammonia with higher values  
 591 of  $f_{\text{storm}}$ . Of course important caveats, among them the fact that our model is purely  
 592 local, that we did not consider radiative heat transport and that convective events  
 593 are prescribed rather than self-consistently determined mean that this mechanism will  
 594 have to be tested within cloud-ensemble models and general circulation models.

595 Our model has a number of important consequences for Jupiter’s deep atmo-  
 596 sphere and interior: First, the equatorial region characterized by a well-mixed am-  
 597 monia concentration, a lack of strong storms and of lightning flashes, should also be  
 598 well-mixed in its water abundance. Its temperature structure is expected to be close  
 599 to a standard moist-adiabat. In contrast, we envision that the mid-latitude regions are  
 600 not well-mixed in water, the increase in both water and ammonia abundance creating  
 601 a region that is on average stably-stratified. The requirement to transport the internal  
 602 heat flux implies that superadiabaticity should be significant, thus explaining, at least  
 603 qualitatively why  $f_{\text{storm}}$  can be significantly larger than unity. This can potentially  
 604 have large implications to explain the internal structure of the planet.

605 The formation of mushballs and evaporative downdrafts should also occur in  
 606 other giant planets in the solar system potentially explaining the low N/C ratio linked  
 607 to the reported low ammonia abundances in the upper tropospheric region (de Pater  
 608 et al., 1991; Fletcher et al., 2011; Irwin et al., 2018; Guillot & Gautier, 2015). The  
 609 latitudinal distribution of ammonia in Saturn, although model-dependent and limited  
 610 to the 1-3 bar region, appears to resemble that obtained for Jupiter with a peak  
 611 in abundance at the equator and much lower values at mid-latitude (Fletcher et al.,  
 612 2011). The same study revealed that the tropospheric abundance of two disequilibrium  
 613 species, arsine and phosphine, instead show a minimum at the equator, raising a  
 614 conundrum (Fletcher et al., 2011). This can now be understood in the framework of  
 615 our model: strong storms, which are located away from the Equatorial Zone in mid-  
 616 latitudes, deliver disequilibrium species from deep levels to elevate their abundance  
 617 relative to the equator, but they tend to remove ammonia at mid-latitudes through  
 618 the mushball process.

619 Finally, we stress that the formation of mushballs lead to the presence of liquid (or  
 620 partially liquid) condensates in a very high region of Jupiter’s atmosphere that would  
 621 otherwise contain only solids and vapor. The consequences of storms on the ammonia  
 622 distribution may be observable by close-up MWR measurements from Juno (Janssen  
 623 et al., 2017) over developing storms. The large-scale mid-latitude North Temperate  
 624 Belt disturbances appear in Jupiter with a cadence of 4 years or so (Sánchez-Lavega et  
 625 al., 2008, 2017) and would be an ideal candidate for an observation by Juno’s full set  
 626 of instrumentation. Planets with hydrogen atmospheres remain crucial laboratories to  
 627 understand atmospheric dynamics and meteorology in a regime in which condensates  
 628 are heavier than the surrounding air (Guillot, 1995).

## 629 Acknowledgments

630 T.G. acknowledges support from the *Centre National d’Etudes Spatiales* and the Japan  
 631 Society for the Promotion of Science. G.O. was supported by funds from NASA dis-  
 632 tributed to the Jet Propulsion Laboratory, California Institute of Technology. J.L. was  
 633 supported by the Juno project through a subcontract from the Southwest Research In-  
 634 stitute. The data used for this article is available at [https://pubdata.space.swri.edu/look/0/7f50acda-](https://pubdata.space.swri.edu/look/0/7f50acda-30f9-43fe-b714-257c71d89404)  
 635 [30f9-43fe-b714-257c71d89404](https://pubdata.space.swri.edu/look/0/7f50acda-30f9-43fe-b714-257c71d89404)

## 636 References

- 637 Bjoraker, G. L., Larson, H. P., & Kunde, V. G. (1986). The Abundance and Distribu-  
 638 tion of Water Vapor in Jupiter’s Atmosphere. *ApJ*, *311*, 1058.
- 639 Blain, D., Fouchet, T., Greathouse, T., Encrenaz, T., Charnay, B., Bézard, B., ...  
 640 Drossart, P. (2018). Mapping of Jupiter’s tropospheric NH<sub>3</sub> abundance using  
 641 ground-based IRTF/TEXES observations at 5 μm. *Icarus*, *314*, 106-120.
- 642 Bolton, S. J., Adriani, A., Adumitroaie, V., Allison, M., Anderson, J., Atreya, S.,  
 643 ... Wilson, R. (2017). Jupiter’s interior and deep atmosphere: The initial  
 644 pole-to-pole passes with the Juno spacecraft. *Science*, *356*(6340), 821-825.
- 645 Brown, S., Janssen, M., Adumitroaie, V., Atreya, S., Bolton, S., Gulikis, S., ... Con-  
 646 nerney, J. (2018). Prevalent lightning sferics at 600 megahertz near Jupiter’s  
 647 poles. *Nature*, *558*(7708), 87-90.
- 648 de Pater, I. (1986). Jupiter’s zone-belt structure at radio wavelengths. II. Compar-  
 649 ison of observations with model atmosphere calculations. *Icarus*, *68*(2), 344-  
 650 365.
- 651 de Pater, I., Dunn, D., Romani, P., & Zahnle, K. (2001). Reconciling Galileo Probe  
 652 Data and Ground-Based Radio Observations of Ammonia on Jupiter. *Icarus*,  
 653 *149*(1), 66-78.
- 654 de Pater, I., Romani, P. N., & Atreya, S. K. (1991). Possible microwave absorption  
 655 by H<sub>2</sub>S gas in Uranus’ and Neptune’s atmospheres. *Icarus*, *91*(2), 220-233.

- 656 de Pater, I., Sault, R. J., Wong, M. H., Fletcher, L. N., DeBoer, D., & Butler, B.  
 657 (2019). Jupiter’s ammonia distribution derived from VLA maps at 3-37 GHz.  
 658 *Icarus*, *322*, 168-191.
- 659 del Genio, A. D., & McGrattan, K. B. (1990). Moist convection and the vertical  
 660 structure and water abundance of Jupiter’s atmosphere. *Icarus*, *84*(1), 29-53.
- 661 Fletcher, L. N., Baines, K. H., Momary, T. W., Showman, A. P., Irwin, P. G. J.,  
 662 Orton, G. S., ... Merlet, C. (2011). Saturn’s tropospheric composition and  
 663 clouds from Cassini/VIMS 4.6-5.1  $\mu\text{m}$  nightside spectroscopy. *Icarus*, *214*(2),  
 664 510-533.
- 665 Friedson, A. J. (2005). Water, ammonia, and H<sub>2</sub>S mixing ratios in Jupiter’s five-  
 666 micron hot spots: A dynamical model. *Icarus*, *177*(1), 1-17.
- 667 García-Melendo, E., Legarreta, J., Sánchez-Lavega, A., Hueso, R., Pérez-Hoyos, S.,  
 668 González, J., ... IOPW Team (2009). The jovian anticyclone BA. I. Motions  
 669 and interaction with the GRS from observations and non-linear simulations.  
 670 *Icarus*, *203*(2), 486-498.
- 671 García-Melendo, E., & Sánchez-Lavega, A. (2001). A Study of the Stability of Jo-  
 672 vian Zonal Winds from HST Images: 1995-2000. *Icarus*, *152*(2), 316-330.
- 673 Gierasch, P. J., Ingersoll, A. P., Banfield, D., Ewald, S. P., Helfenstein, P., Simon-  
 674 Miller, A., ... Galileo Imaging Team (2000). Observation of moist convection  
 675 in Jupiter’s atmosphere. *Nature*, *403*(6770), 628-630.
- 676 Giles, R. S., Fletcher, L. N., Irwin, P. G. J., Orton, G. S., & Sinclair, J. A. (2017).  
 677 Ammonia in Jupiter’s Troposphere From High-Resolution 5  $\mu\text{m}$  Spectroscopy.  
 678 *Geophys. Res. Lett.*, *44*(21), 10,838-10,844.
- 679 Grassi, D., Adriani, A., Mura, A., Dinelli, B. M., Sindoni, G., Turrini, D., ...  
 680 Amoroso, M. (2017). Preliminary results on the composition of Jupiter’s  
 681 troposphere in hot spot regions from the JIRAM/Juno instrument. *Geo-*  
 682 *phys. Res. Lett.*, *44*(10), 4615-4624.
- 683 Grassi, D., Adriani, A., Mura, A., Fletcher, L. N., Lunine, J. I., Orton, G. S.,  
 684 ... Turrini, D. (2020). On the spatial distribution of minor species in  
 685 Jupiter’s troposphere as inferred from Juno JIRAM data. *Submitted to Geo-*  
 686 *phys. Res. Lett.*
- 687 Guillot, T. (1995). Condensation of Methane, Ammonia, and Water and the Inhibi-  
 688 tion of Convection in Giant Planets. *Science*, *269*(5231), 1697-1699.
- 689 Guillot, T. (2005). THE INTERIORS OF GIANT PLANETS: Models and Out-  
 690 standing Questions. *Annual Review of Earth and Planetary Sciences*, *33*, 493-  
 691 530.
- 692 Guillot, T., & Gautier, D. (2015). Giant planets. In G. Schubert & T. Spohn (Eds.),  
 693 *Treatise in geophysics, 2nd edition* (Vol. 269).
- 694 Guillot, T., Gautier, D., Chabrier, G., & Mosser, B. (1994). Are the Giant Planets  
 695 Fully Convective? *Icarus*, *112*(2), 337-353.
- 696 Guillot, T., Stevenson, D. J., Hubbard, W. B., & Saumon, D. (2004). The interior of  
 697 Jupiter. In F. Bagenal, T. E. Dowling, & W. B. McKinnon (Eds.), *Jupiter. the*  
 698 *planet, satellites and magnetosphere* (p. 35-57).
- 699 Hanel, R., Conrath, B., Herath, L., Kunde, V., & Pirraglia, J. (1981). Albedo, in-  
 700 ternal heat, and energy balance of Jupiter: preliminary results of the voyager  
 701 infrared investigation. *J. Geophys. Res.*, *86*(A10), 8705-8712.
- 702 Holton, J. R. (1992). *An introduction to dynamic meteorology*.
- 703 Ingersoll, A. P., Adumitroaie, V., Allison, M. D., Atreya, S., Bellotti, A. A., Bolton,  
 704 S. J., ... Steffes, P. G. (2017). Implications of the ammonia distribution on  
 705 Jupiter from 1 to 100 bars as measured by the Juno microwave radiometer.  
 706 *Geophys. Res. Lett.*, *44*(15), 7676-7685.
- 707 Ingersoll, A. P., & Porco, C. C. (1978). Solar heating and internal heat flow on  
 708 Jupiter. *Icarus*, *35*(1), 27-43.
- 709 Irwin, P. G. J., Toledo, D., Garland, R., Teanby, N. A., Fletcher, L. N., Orton,  
 710 G. A., & Bézard, B. (2018). Detection of hydrogen sulfide above the clouds in

- 711 Uranus’s atmosphere. *Nature Astronomy*, *2*, 420-427.
- 712 Janssen, M. A., Oswald, J. E., Brown, S. T., Gulkis, S., Levin, S. M., Bolton, S. J.,  
713 ... Wang, C. C. (2017). MWR: Microwave Radiometer for the Juno Mission  
714 to Jupiter. *Space Sci. Rev.*, *213*(1-4), 139-185.
- 715 Leconte, J., Selsis, F., Hersant, F., & Guillot, T. (2017). Condensation-inhibited  
716 convection in hydrogen-rich atmospheres . Stability against double-diffusive  
717 processes and thermal profiles for Jupiter, Saturn, Uranus, and Neptune.  
718 *A&A*, *598*, A98.
- 719 Li, C., & Chen, X. (2019). Simulating Nonhydrostatic Atmospheres on Planets  
720 (SNAP): Formulation, Validation, and Application to the Jovian Atmosphere.  
721 *ApJS*, *240*(2), 37.
- 722 Li, C., Ingersoll, A., Janssen, M., Levin, S., Bolton, S., Adumitroaie, V., ...  
723 Williamson, R. (2017). The distribution of ammonia on Jupiter from a pre-  
724 liminary inversion of Juno microwave radiometer data. *Geophys. Res. Lett.*,  
725 *44*(11), 5317-5325.
- 726 Li, C., & Ingersoll, A. P. (2015). Moist convection in hydrogen atmospheres and the  
727 frequency of Saturn’s giant storms. *Nature Geoscience*, *8*(5), 398-403.
- 728 Li, L., Jiang, X., West, R. A., Gierasch, P. J., Perez-Hoyos, S., Sanchez-Lavega, A.,  
729 ... Schmude, R. W. (2018). Less absorbed solar energy and more internal heat  
730 for Jupiter. *Nature Communications*, *9*, 3709.
- 731 Lindal, G. F. (1992). The Atmosphere of Neptune: an Analysis of Radio Occultation  
732 Data Acquired with Voyager 2. *AJ*, *103*, 967.
- 733 Lindal, G. F., Wood, G. E., Levy, G. S., Anderson, J. D., Sweetnam, D. N., Hotz,  
734 H. B., ... Croft, T. A. (1981). The atmosphere of Jupiter: an analysis of the  
735 Voyager radio occultation measurements. *J. Geophys. Res.*, *86*(A10), 8721-  
736 8727.
- 737 Lodders, K. (2003). Solar System Abundances and Condensation Temperatures of  
738 the Elements. *ApJ*, *591*(2), 1220-1247.
- 739 Lunine, J. I., & Hunten, D. M. (1987). Moist convection and the abundance of water  
740 in the troposphere of Jupiter. *Icarus*, *69*(3), 566-570.
- 741 Magalhaes, J. A., Seiff, A., & Young, R. E. (2002). The Stratification of Jupiter’s  
742 Troposphere at the Galileo Probe Entry Site. *Icarus*, *158*(2), 410-433.
- 743 Markham, S., & Stevenson, D. (2018). Excitation mechanisms for Jovian seismic  
744 modes. *Icarus*, *306*, 200-213.
- 745 Niemann, H. B., Atreya, S. K., Carignan, G. R., Donahue, T. M., Haberman, J. A.,  
746 Harpold, D. N., ... Way, S. H. (1998). The composition of the Jovian at-  
747 mosphere as determined by the Galileo probe mass spectrometer. *J. Geo-  
748 phys. Res.*, *103*(E10), 22831-22846.
- 749 Ortiz, J. L., Orton, G. S., Friedson, A. J., Stewart, S. T., Fisher, B. M., & Spencer,  
750 J. R. (1998). Evolution and persistence of 5- $\mu$ m hot spots at the Galileo probe  
751 entry latitude. *J. Geophys. Res.*, *103*(E10), 23051-23069.
- 752 Palotai, C., & Dowling, T. E. (2008). Addition of water and ammonia cloud micro-  
753 physics to the EPIC model. *Icarus*, *194*(1), 303-326.
- 754 Palotai, C., Dowling, T. E., & Fletcher, L. N. (2014). 3D Modeling of interac-  
755 tions between Jupiter’s ammonia clouds and large anticyclones. *Icarus*, *232*,  
756 141-156.
- 757 Porco, C. C., West, R. A., McEwen, A., Del Genio, A. D., Ingersoll, A. P., Thomas,  
758 P., ... Vasavada, A. R. (2003). Cassini Imaging of Jupiter’s Atmosphere,  
759 Satellites, and Rings. *Science*, *299*(5612), 1541-1547.
- 760 Rafkin, S. C. R., & Barth, E. L. (2015). Environmental control of deep convective  
761 clouds on Titan: The combined effect of CAPE and wind shear on storm dy-  
762 namics, morphology, and lifetime. *Journal of Geophysical Research (Planets)*,  
763 *120*(4), 739-759.
- 764 Roos-Serote, M., Atreya, S. K., Wong, M. K., & Drossart, P. (2004). On the water  
765 abundance in the atmosphere of Jupiter. *Planet. Space Sci.*, *52*(5-6), 397-414.

- 766 Sánchez-Lavega, A., Orton, G. S., Hueso, R., García-Melendo, E., Pérez-Hoyos, S.,  
 767 Simon-Miller, A., ... Pujic, Z. (2008). Depth of a strong jovian jet from a  
 768 planetary-scale disturbance driven by storms. *Nature*, *451*(7177), 437-440.
- 769 Sánchez-Lavega, A., Rogers, J. H., Orton, G. S., García-Melendo, E., Legarreta, J.,  
 770 Colas, F., ... Wesley, A. (2017). A planetary-scale disturbance in the most  
 771 intense Jovian atmospheric jet from JunoCam and ground-based observations.  
 772 *Geophys. Res. Lett.*, *44*(10), 4679-4686.
- 773 Seiff, A., Kirk, D. B., Knight, T. C. D., Young, R. E., Mihalov, J. D., Young, L. A.,  
 774 ... Atkinson, D. (1998). Thermal structure of Jupiter's atmosphere near  
 775 the edge of a 5- $\mu$ m hot spot in the north equatorial belt. *J. Geophys. Res.*,  
 776 *103*(E10), 22857-22890.
- 777 Showman, A. P., & Dowling, T. E. (2000). Nonlinear Simulations of Jupiter's 5-  
 778 Micron Hot Spots. *Science*, *289*(5485), 1737-1740.
- 779 Showman, A. P., & Ingersoll, A. P. (1998). Interpretation of Galileo Probe Data and  
 780 Implications for Jupiter's Dry Downdrafts. *Icarus*, *132*(2), 205-220.
- 781 Sugiyama, K., Nakajima, K., Odaka, M., Kuramoto, K., & Hayashi, Y. Y. (2014).  
 782 Numerical simulations of Jupiter's moist convection layer: Structure and dy-  
 783 namics in statistically steady states. *Icarus*, *229*, 71-91.
- 784 Tollefson, J., Wong, M. H., Pater, I. d., Simon, A. A., Orton, G. S., Rogers, J. H.,  
 785 ... Marcus, P. S. (2017). Changes in Jupiter's Zonal Wind Profile preceding  
 786 and during the Juno mission. *Icarus*, *296*, 163-178.
- 787 Wong, M. H., Mahaffy, P. R., Atreya, S. K., Niemann, H. B., & Owen, T. C. (2004).  
 788 Updated Galileo probe mass spectrometer measurements of carbon, oxygen,  
 789 nitrogen, and sulfur on Jupiter. *Icarus*, *171*(1), 153-170.
- 790 Yair, Y., Levin, Z., & Tzivion, S. (1995). Microphysical processes and dynamics of a  
 791 Jovian thundercloud. *Icarus*, *114*(2), 278-299.